NANO LETTERS

Letter

pubs.acs.org/NanoLett

Adhesion, Stiffness, and Instability in Atomically Thin MoS_2 Bubbles

David Lloyd,[†] Xinghui Liu,[‡] Narasimha Boddeti,[‡] Lauren Cantley,[†] Rong Long,[‡] Martin L. Dunn,[§] and J. Scott Bunch*[,†,∥]

[†]Department of Mechanical Engineering, Boston University, Boston, Massachusetts 02215 United States

[‡]Department of Mechanical Engineering, University of Colorado, Boulder, Colorado 80309 United States

[§]Singapore University of Technology and Design, Singapore 487372

[∥]Boston University, Division of Materials Science and Engineering, Brookline, Massachusetts 02446 United States

Supporting Information

ABSTRACT: We measured the work of separation of single and few-layer MoS_2 membranes from a SiO_x substrate using a mechanical blister test and found a value of 220 ± 35 mJ/m^2. Our measurements were also used to determine the 2D Young's modulus (E_{2D}) of a single MoS_2 layer to be 160 ± 40 N/m. We then studied the delamination mechanics of pressurized MoS_2 bubbles, demonstrating both stable and unstable transitions between the bubbles' laminated and delaminated states as the bubbles were inflated. When they were deflated, we observed edge pinning and a snap-in transition that are not accounted for by the previously reported models. We attribute this result to adhesion hysteresis and use our results to estimate the work of adhesion of our membranes to be 42 ± 20 mJ/m^2.

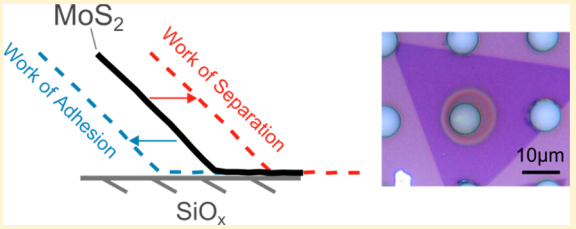

KEYWORDS: *Adhesion, MoS_2, adhesion hysteresis, Young's modulus, friction, bubble*

Adhesive forces play an important role in shaping the mechanical behavior of atomically thin materials such as graphene or molybdenum disulfide, MoS_2. These forces keep the material clamped to the substrate, and also influence how the membrane folds,[1] slides,[2] and peels.[3] An understanding of adhesion in these materials is important in the fabrication of nanoelectromechanical systems,[4] flexible electronic devices,[5] graphene origami,[1,6] graphene separation membranes,[7] and stacked heterostructures formed from 2D materials. Atomically thin crystals may also provide a fruitful system in which to study novel features of friction and adhesion present only at the nanoscale.[2,8−10] In terms of device performance, adhesive forces determine the maximum strain 2D materials can support, which is important in designing stretchable electronic devices[11] and pressure sensors.[12]

The study of bubbles formed by atomically thin sheets has proven to be useful for discovering the adhesive and mechanical properties of these materials and has allowed measurements of the adhesion energies,[13] friction coefficient,[14] and Young's modulus of graphene and other 2D materials.[15] In particular, Koenig et al. used a mechanical blister test to measure the adhesion energy between graphene and SiO_x of ∼450 mJ/m^2. Like graphene, atomically thin MoS_2 is a mechanically exceptional material,[16] while also being piezoelectric[11,17] and a direct gap semiconductor with a highly strain sensitive band gap.[18−21] A good understanding of the mechanical stiffness and adhesion to the substrate is therefore of particular importance to this material that has applications involving the interplay between adhesive and tensile forces.

In this paper, we measure the work of separation (sometimes referred to as the adhesion energy) between MoS_2 and the substrate by employing the same geometry as used in our previous work[7,13,22] in which we suspend mechanically exfoliated or chemical vapor deposition (CVD) grown membranes over cylindrical microcavities etched into a silicon oxide (SiO_x) substrate (Figure 1a,b). The devices are then placed in a pressure chamber filled with a gas of pressure p_0, which gradually leaks into the cavities through the SiO_x substrate until the internal pressure p_{int} reaches that of the chamber ($p_{int} = p_0$). We used either N_2, Ar, H_2, or He gas that allowed us to choose a convenient leak rate of the gas into the microcavities. When the devices are removed from the pressure chamber the p_{int} is greater than the external pressure (p_{ext} = 1 atm), and this pressure difference ($\Delta p = p_{int} - p_{ext} > 0$) causes the membrane to bulge up (Figure 1c,d). For each charging pressure p_0 we measure the deflection δ and radius a of the bubble using an atomic force microscope (AFM) after which the devices are returned to the pressure chamber at a higher p_0 and the process is repeated. We fabricated devices of 1−3 layer thickness by mechanical exfoliation and made monolayer devices from CVD grown MoS_2 using a PMMA transfer method (see Supporting Information for details). We transferred six different growths to produce CVD samples *N*1−6

Received: April 24, 2017
Revised: July 22, 2017
Published: August 1, 2017

DOI: 10.1021/acs.nanolett.7b01735
Nano Lett. XXXX, XXX, XXX−XXX

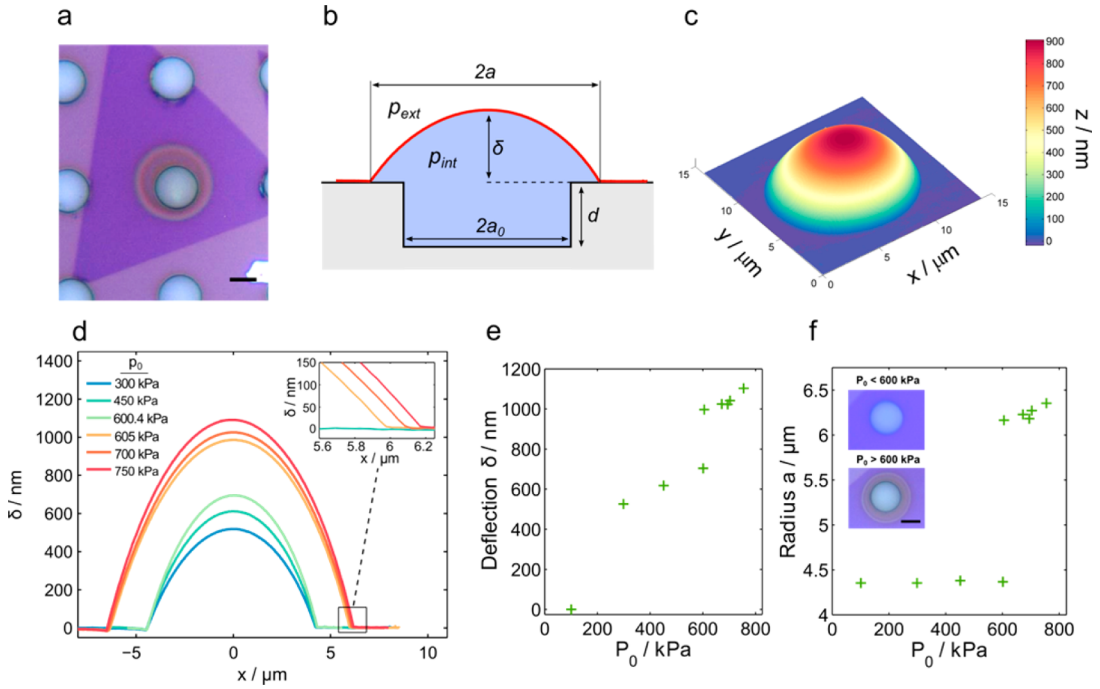

Figure 1. (a) Microscope image of a delaminated device (scale bar is 5 μm). (b) Device schematic. (c) AFM image and (d) AFM cross sections. (e) Deflection δ and (f) radius a plotted against input pressure p_0. Inset microscope images show a device before and after snap-out (scale bar is 5 μm).

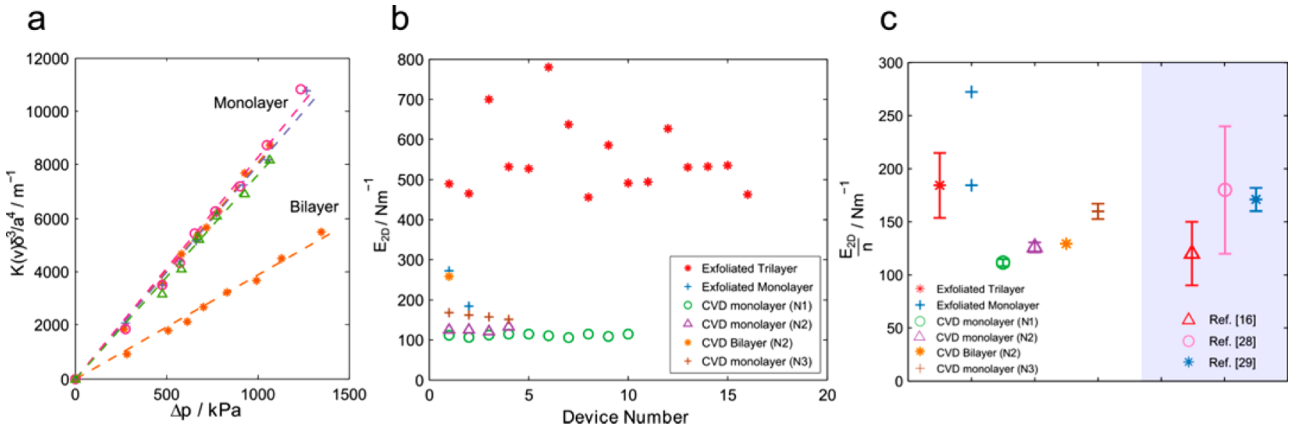

Figure 2. (a) Plots for CVD monolayer and bilayer devices (different symbols/colors represent each device), with linear fits (dashed lines) used to find E_{2D}. (b) E_{2D} for each device in our exfoliated samples, and three of our CVD samples ($N1-3$). (c) E_{2D} divided by number of layers n for each sample. Data points and error bars represent the mean and standard deviation respectively for each sample. Results from nanoindentation measurements in refs 16, 28, and 29 are plotted for comparison.

with each containing many individual devices. The SiO_x substrates were O_2 plasma cleaned prior to transfer.

As can be seen in Figure 1d–f, increasing p_0 causes δ to increase with a initially remaining pinned at the radius of the cylindrical microcavity, a_0. After a critical pressure is reached ($p_0 \sim 600$ kPa), the force from the pressure difference across the membrane overcomes the adhesive forces keeping the membrane clamped to the substrate, and delamination occurs in the form of a snap-out transition of the radius from 4.4 to 6 μm. After the snap-out transition, both a and δ continue to gradually increase as p_0 is increased.

We begin by using our values for p_0, δ, and a to determine the Young's modulus of MoS_2 with a formula developed in Hencky's model for clamped pressurized membranes,[23] which relates the pressure difference across the membrane Δp to the deflection δ and radius a by the formula

$$\Delta p = \frac{K(\nu)E_{2D}\delta^3}{a^4} \quad (1)$$

with a Poisson's ratio $\nu = 0.29$,[16] numerical constant $K(\nu) = 3.54$ and a two-dimensional Young's modulus E_{2D} equal to the bulk Young's modulus multiplied by the thickness of the material. The pressure difference, Δp, is calculated from p_0 by assuming isothermal expansion of a fixed number of ideal gas molecules from the initial volume of the cavity (V_0) to its final volume ($V_0 + V_b$), such that $p_0V_0 = p_{int}(V_0 + V_b)$. From Hencky's model, the volume created beneath the bubble can be found from the device geometry using the expression $V_b = C(\nu)\pi a^2\delta$, and a numerical constant $C(\nu) = 0.522$.

We measured the E_{2D} of 3 CVD samples ($N1-3$) and of exfoliated monolayer and trilayer flakes containing 2 and 16 devices, respectively. Figure 2a shows a plot of Δp against

DOI: 10.1021/acs.nanolett.7b01735
Nano Lett. XXXX, XXX, XXX−XXX

$K(\nu)\delta^3/a^4$ for each of our CVD monolayer and bilayer devices in sample *N*2, including linear fits which are used to determine E_{2D} for each device. The E_{2D} of each device in these samples is plotted in Figure 2b. In Figure 2c, we plot the mean E_{2D} for each sample divided by the number of layers n in the membranes in order to compare estimates for the E_{2D} of a single MoS_2 layer. Error bars represent the standard deviation.

For our exfoliated devices we find an average E_{2D} per layer of 190 ± 35 N/m, and for our CVD grown MoS_2 monolayers we find an average E_{2D} of 128 ± 20 N/m. There is a low variance of E_{2D} within each CVD grown sample, however, there is a significant difference between the average E_{2D} for each CVD sample. The discrepancy between CVD and exfoliated samples and among different CVD samples may be due to differences in defect densities[24,25] which occur during CVD growth, as an increased sulfur vacancy density[26] is predicted to lower E_{2D} in MoS_2.[27] The average of all our exfoliated and CVD grown samples is 160 ± 40 N/m, which falls within the same range of values as found in previous studies,[16,28,29] which we plot in Figure 2c for comparison.

We next determined the work of separation, Γ_{sep}, using our values for p_0, δ, and a and a free energy model described in detail by others.[30,31] Briefly, we can write the total free energy of the system F as

$$F = \frac{(p_{int} - p_{ext})V_b}{4} + \Gamma\pi(a^2 - a_0^2) - p_0V_0 \ln\left[\frac{V_0 + V_b}{V_0}\right] + p_{ext}V_b \quad (2)$$

where V_0 is the initial volume of the cavity, V_b is the additional volume created as the bubble expands. Γ is the adhesion energy, which is equal to Γ_{sep} in the case of delamination. The first two terms represent the elastic strain energy and the work to separate the membrane from the substrate respectively, and the final two terms account for the isothermal expansion of the gas.

When a device is removed from the pressure chamber, the bubble volume expands until the free energy of the system F reaches a local minimum. We minimize F with respect to a by setting $dF/da = 0$ and using the relationship $p_0V_0 = p_{int}(V_0 + V_b)$. This yields the expression for the work of separation

$$\Gamma_{sep} = \frac{5C}{4}\left(\frac{p_0V_0}{V_0 + V_b(\delta, a)} - p_{ext}\right)\delta \quad (3)$$

with the constant $C(\nu) = 0.522$ for $\nu = 0.29$.[16] Using this expression, we can determine Γ_{sep} of each device using the charging pressure of the pressure chamber p_0, and δ and a of the bubble measured using an AFM. We can also substitute the pressure terms in eq 3 with Hencky's result in eq 1 which yields

$$\Gamma_{sep} = \frac{5}{4}CKE_{2D}\left(\frac{\delta}{a}\right)^4 \quad (4)$$

which holds for all devices which have started to delaminate ($a > a_0$). This allows Γ_{sep} to be determined from δ and a without knowing p_0, which avoids the long waiting times required for devices to reach equilibrium in the pressure chamber. For our exfoliated devices, we calculated Γ_{sep} using eq 4 (using the mean value of E_{2D} = 190 N/m per layer we found earlier for exfoliated samples) and used eq 3 to calculate Γ_{sep} for our CVD devices where p_0 was well-known.

We find no significant difference in Γ_{sep} between single and few layer samples, or CVD and exfoliated samples (Figure 3).

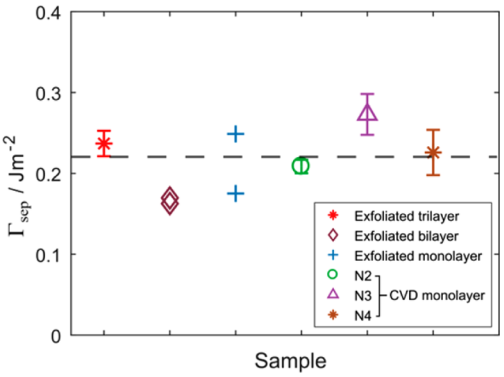

Figure 3. Work of separation of membranes of 1−3 layer thickness. The data includes measurements of CVD monolayer devices from three separate growths and transfers (*N*2−4). Several devices are measured per sample, with data points and error bars representing the means and standard deviations, respectively. For samples with fewer than three measurements, the data points represent each device measured. The dashed line marks the mean of the six samples.

By averaging over all samples, we find the mean work of separation to be Γ_{sep} = 220 ± 35 mJ/m^2, which is close to the value of 170 ± 30 mJ/m^2 measured for many layer MoS_2[32] and is in the same range of values as found for graphene.[13,33−36]

The devices shown in Figure 1d−f exhibit unstable delamination, whereby a discontinuously increases from the initial radius a_0 when $p_0 \gtrsim 600$ kPa. The etched depth of the microcavities in that case was d = 1500 nm. We also fabricated devices with cavity depths of d = 650 nm, and again performed measurements of δ and a at increasing p_0 (Figure S9) using the method described earlier. With this cavity depth, the devices show no snap-out transition and rather stably delaminate with a continuously increasing from a_0. The difference in behavior in these two cases has been observed and modeled by others,[31,37] and Bodetti et al. found that the transition from unstable to stable delamination occurs when the parameter $S = 2V_b/V_0$ satisfies the condition $S > 1$ just before the point of delamination.[31] Reducing the well depth decreases the volume of the cavity relative to the volume of the bubble, which increases S. By making various device geometries and finding S from AFM measurements we confirmed empirically that this transition occurs in the range $0.74 < S < 1.11$, and we obtained the same value for Γ_{sep} for both stable and unstable delamination (see Supporting Information for details).

After the devices with d = 1500 nm (on sample *N*2) had been delaminated to their largest radii, they were left out in ambient conditions to deflate over the course of ∼48 h. During this time AFM scans captured δ and a as the number of gas molecules N decreases from the initial value of N_0 ($= p_0V_0/k_bT$). AFM cross sections of a bubble are shown in Figure 4a during the inflation (increasing N_0) and deflation (decreasing N) of the device. Initially as the device is inflated, δ increases and a remains pinned at a_0. When $p_0 \gtrsim 600$ kPa the snap-out transition occurs and a jumps to a larger value, after which both a and δ increase together as N_0 increases. When devices are left to deflate, δ decreases from an initial value of δ_0, however a now does not change from its radius at the beginning of deflation, which we refer to as the "pinned radius" a_p. After the deflection of the devices reaches a critical value $\delta = \delta_c$, the devices undergo a snap-in transition where the radius jumps from a_p to a_0 and δ continues to decrease to zero. Values for δ and a throughout this process are shown in Figure 4b, which

DOI: 10.1021/acs.nanolett.7b01735
Nano Lett. XXXX, XXX, XXX−XXX

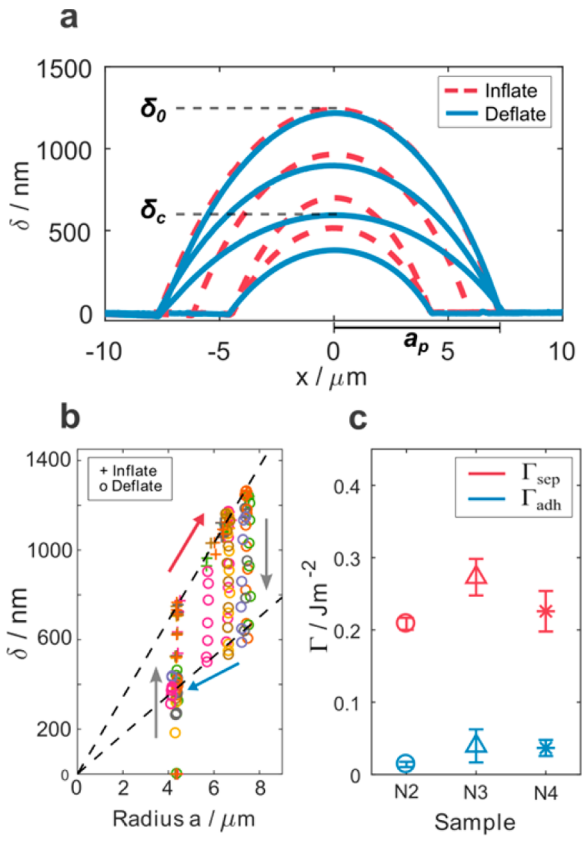

Figure 4. (a) AFM cross sections of a device during inflation (increasing N) and deflation (decreasing N). Arrows mark the snap transitions. (b) δ and a of devices during inflation and deflation. Different colors represent different devices on sample $N2$. More data can be found in the Supporting Information which is not shown here for reasons of clarity. Red and blue arrows mark snap-out and snap-ins, respectively. The upper and lower dashed lines correspond to solutions to eq 4 and eq 5 respectively. (c) A comparison between the works of separation and adhesion for samples $N2$–4. Data points and error bars represent the means and standard deviations respectively of all the devices measured on each sample.

shows devices deflating at a number of different a_p. Videos of the snap-out and snap-in transitions can be seen in the Supporting Information.

We can interpret this using the result derived in eq 4, which requires that after delamination the ratio δ/a remains constant with the magnitude of this ratio being proportional to $\Gamma_{sep}^{1/4}$. We plot the line corresponding to this formula in Figure 4b (upper dashed line) with the values of E_{2D} and Γ_{sep} determined earlier, and find our data for increasing N_0 follows this trend very well.

This formula is independent of whether N is increasing or decreasing, so when our devices are left to deflate we should expect δ and a to return along the same path as during inflation described by eq 4. As can be seen in Figure 4a, however, there is a significant difference in the geometry of the bubbles during inflation and deflation, which suggests some element of our system is irreversible.

We attribute the difference between inflation and deflation we see in our data to the widely observed phenomenon of adhesion hysteresis,[34,38,39] whereby the energy required to separate the membrane from the surface Γ_{sep} is greater than the energy returned to the system as the membrane readheres Γ_{adh} with $\Gamma_{adh} < \Gamma_{sep}$. After making this simple modification (see Supporting Information for more details), our model now predicts that the device should remain pinned at radius a_p until a snap-in transition occurs at a critical deflection determined by

$$\Gamma_{adh} = \frac{5}{4} C K E_{2D} \left(\frac{\delta_c}{a_p} \right)^4 \quad (5)$$

We perform a linear fit of our measurements of δ_c and a_p (lower dashed line in Figure 4b) that yields an estimate of the work of adhesion for this sample to be $\Gamma_{adh} = 14 \pm 5$ mJ/m^2. Multiple measurements of Γ_{adh} with the same device show that this measurement is repeatable over many cycles (Figure S3b in the Supporting Information). We performed measurements on a total of five CVD grown samples ($N2$–6) and found the mean work of adhesion for all our samples to be 42 ± 20 mJ/m^2 with $\Gamma_{adh} < \Gamma_{sep}$ in every device. Figure 4c shows a comparison between the works of separation and adhesion for three of these samples ($N2$–4). Γ_{adh} varied noticeably between samples with sample means falling in the range 14–63 mJ/m^2 (Figure S5 in the Supporting Information).

Our measurements of Γ_{adh} show that as little as one-tenth of the energy required to separate the membrane from the substrate ($\Gamma_{sep} \sim 220$ mJ/m^2) is recovered as the membrane at the edge of the bubble readheres to the substrate. We used Raman spectroscopy to measure the membrane strain distribution around our devices before and after snap-in (see Supporting Information for details); we found that while some energy was dissipated in the form of residual strain transferred to the membrane, this can only account for <10% of the dissipation that produces a difference between Γ_{adh} and Γ_{sep}. This strain may also dissipate some energy through frictional sliding as the membrane changes its length on the surface of the substrate.[14]

Adhesion hysteresis is a commonly observed phenomenon[40] which has previously been observed in nanoindentation measurements of graphene,[34] and the fraction of the energy dissipated in our system is comparable with the hysteresis observed in elastomers.[41] The behavior of our devices is also analogous to the related phenomenon of contact angle hysteresis seen in liquid bubbles,[39] and constant contact area pinning during unloading has been seen previously between two adhered solid spheres.[42] Surface roughness and chemical heterogeneity on the surface can produce contact angle and adhesion hysteresis,[40,43] and a further contribution in our system could be the finite time over which deflation occurs. This could mean that the membrane does not have time during the measurement to reconform fully to the surface or remake the bonds which were made before the device delaminated.[44,45] This would result in the system being in a transient nonequilibrium state during the measurement, which is a common cause of thermodynamic irreversibility and adhesion hysteresis.[40,46,47] Our method of finding Γ_{sep} also involves subjecting the membranes to high external pressures prior to measurement, which could improve their conformation to the substrate and thereby enhance Γ_{sep} relative to Γ_{adh}.

We have measured the work of separation of single and few layer MoS_2 fabricated by CVD and mechanical exfoliation and found a value of $\Gamma_{sep} = 220 \pm 35$ J/m^2. We also measured the Young's modulus and found that $E_{2D} = 160 \pm 40$ N/m for a single MoS_2 layer. Bulge testing provides a complementary method to nanoindentation to determine E_{2D}, and our results are in the same range of values as reported in previous studies. We demonstrated snap-out and snap-in instabilities, which

DOI: 10.1021/acs.nanolett.7b01735
Nano Lett. XXXX, XXX, XXX−XXX

mechanically amplify small changes in pressure and could be used for pressure sensing. Finally, we observed bubble edge pinning, analogous to contact angle hysteresis observed in liquids, and used Raman spectroscopy to provide evidence that the trapping of strain energy after the snap-in transition can account for some but not all of the hysteresis. We measured a Γ_{adh} that was significantly lower than Γ_{sep}, which may affect the performance of nanomechanical switches made from atomically thin materials.[48,49] The distinction between Γ_{adh} and Γ_{sep} we have observed here is an important consideration in the analysis of bubbles formed under atomically thin crystals[15,50,51] and in the design of folded 3D structures made from 2D sheets.[1,6]

■ ASSOCIATED CONTENT

Supporting Information

The Supporting Information is available free of charge on the ACS Publications website at DOI: 10.1021/acs.nanolett.7b01735.

Details of CVD growth and characterization, the effect of membrane pretension, the full set of work of adhesion and separation data, the free energy model including the effect of adhesion hysteresis, contact angle measurements of a bubble during deflation, the trapping of strain around the edge of the devices, the effect of membrane slipping on our E_{2D} calculations, data from devices which exhibit stable delamination, additional measurements of deflating devices, the full set of Young's modulus data (PDF)

Video 1 of the snap transitions (AVI)

Video 2 of the snap transitions (AVI)

■ AUTHOR INFORMATION

Corresponding Author

*E-mail: bunch@bu.edu.

ORCID

David Lloyd: 0000-0002-9828-6152

Notes

The authors declare no competing financial interest.

■ ACKNOWLEDGMENTS

This work was funded by the National Science Foundation (NSF), Grant 1054406 (CMMI: CAREER, Atomic Scale Defect Engineering in Graphene Membranes), a grant to L.C. by the NSF Graduate Research Fellowship Program under Grant DGE-1247312, and a BUnano Cross-Disciplinary Fellowship to D.L. We thank Chuanhua Duan for use of the high speed camera.

■ REFERENCES

(1) Cranford, S.; Sen, D.; Buehler, M. J. *Appl. Phys. Lett.* **2009**, *95*, 123121.

(2) Li, S.; Li, Q.; Carpick, R. W.; Gumbsch, P.; Liu, X. Z.; Ding, X.; Sun, J.; Li, J. *Nature* **2016**, *539*, 541.

(3) Annett, J.; Cross, G. L. W. *Nature* **2016**, *535* (7611), 271–275.

(4) Bunch, J. S.; Van Der Zande, A. M.; Verbridge, S. S.; Frank, I. W.; Tanenbaum, D. M.; Parpia, J. M.; Craighead, H. G.; McEuen, P. L. *Science* **2007**, *315*, 490–493.

(5) Akinwande, D.; Petrone, N.; Hone, J. *Nat. Commun.* **2014**, *5*, 5678.

(6) Ebbesen, T. W.; Hiura, H. *Adv. Mater.* **1995**, *7* (6), 582–586.

(7) Koenig, S. P.; Wang, L.; Pellegrino, J.; Bunch, J. S. *Nat. Nanotechnol.* **2012**, *7*, 728–732.

(8) Carpick, R. W.; Salmeron, M. *Chem. Rev.* **1997**, *97*, 1163–1194.

(9) Lee, C.; Li, Q.; Kalb, W.; Liu, X.; Berger, H.; Carpick, R. W.; Hone, J. *Science* **2010**, *328*, 76–80.

(10) Koren, E.; Lörtscher, E.; Rawlings, C.; Knoll, A. W.; Duerig, U. *Science* **2015**, *348* (6235), 679–683.

(11) Wu, W.; Wang, L.; Li, Y.; Zhang, F.; Lin, L.; Niu, S.; Chenet, D.; Zhang, X.; Hao, Y.; Heinz, T. F.; Hone, J.; Wang, Z. L. *Nature* **2014**, *514* (7523), 470–474.

(12) Smith, A. D.; Niklaus, F.; Paussa, A.; Schröder, S.; Fischer, A. C.; Sterner, M.; Wagner, S.; Vaziri, S.; Forsberg, F.; Esseni, D.; Östling, M.; Lemme, M. C. *ACS Nano* **2016**, *10*, 9879–9886.

(13) Koenig, S. P.; Boddeti, N. G.; Dunn, M. L.; Bunch, J. S. *Nat. Nanotechnol.* **2011**, *6* (9), 543–546.

(14) Kitt, A. L.; Qi, Z.; Remi, S.; Park, H. S.; Swan, A. K.; Goldberg, B. B. *Nano Lett.* **2013**, *13*, 2605–2610.

(15) Khestanova, E.; Fumagalli, L.; Geim, A. K.; Grigorieva, I. V. *Nat. Commun.* **2016**, *7*, 12587.

(16) Cooper, R. C.; Lee, C.; Marianetti, C. A.; Wei, X.; Hone, J.; Kysar, J. W. *Phys. Rev. B: Condens. Matter Mater. Phys.* **2013**, *87* (3), 035423.

(17) Zhu, H.; Wang, Y.; Xiao, J.; Liu, M.; Xiong, S.; Wong, Z. J.; Ye, Z.; Ye, Y.; Yin, X.; Zhang, X. *Nat. Nanotechnol.* **2014**, *10* (2), 151–155.

(18) He, K.; Poole, C.; Mak, K. F.; Shan, J. *Nano Lett.* **2013**, *13* (6), 2931–2936.

(19) Conley, H. J.; Wang, B.; Ziegler, J. I.; Haglund, R. F.; Pantelides, S. T.; Bolotin, K. I. *Nano Lett.* **2013**, *13* (8), 3626–3630.

(20) Castellanos-Gomez, A.; Roldan, R.; Cappelluti, E.; Buscema, M.; Guinea, F.; Van Der Zant, H. S. J.; Steele, G. A. *Nano Lett.* **2013**, *13* (11), 5361–5366.

(21) Lloyd, D.; Liu, X.; Christopher, J. W.; Cantley, L.; Wadehra, A.; Kim, B. L.; Goldberg, B. B.; Swan, A. K.; Bunch, J. S. *Nano Lett.* **2016**, *16*, 5836–5841.

(22) Bunch, J. S.; Verbridge, S. S.; Alden, J. S.; Van Der Zande, A. M.; Parpia, J. M.; Craighead, H. G.; McEuen, P. L. *Nano Lett.* **2008**, *8* (8), 2458–2462.

(23) Fichter, W. *NASA Technol. Pap.* **1997**, *3658*, 1–24.

(24) Zandiatashbar, A.; Lee, G.; An, S. J.; Lee, S.; Mathew, N.; Terrones, M.; Hayashi, T.; Picu, C. R.; Hone, J.; Koratkar, N. *Nat. Commun.* **2014**, *5*, 3186.

(25) López-Polín, G.; Gómez-Navarro, C.; Parente, V.; Katsnelson, M. I.; Pérez-Murano, F.; Gómez-Herrero, J. *Nat. Phys.* **2014**, *11*, 26–31.

(26) Hong, J.; Hu, Z.; Probert, M.; Li, K.; Lv, D.; Yang, X.; Gu, L.; Mao, N.; Feng, Q.; Xie, L.; Zhang, J.; Wu, D.; Zhang, Z.; Jin, C.; Ji, W.; Wu, D.; Zhang, Z.; Jin, C.; Ji, W.; Zhang, X.; Yuan, J.; Zhang, Z. *Nat. Commun.* **2015**, *6*, 6293.

(27) Gan, Y.; Zhao, H. *Phys. Lett. A* **2014**, *378* (38–39), 2910–2914.

(28) Bertolazzi, S.; Brivio, J.; Kis, A. *ACS Nano* **2011**, *5* (12), 9703–9709.

(29) Liu, K.; Yan, Q.; Chen, M.; Fan, W.; Sun, Y.; Suh, J.; Fu, D.; Lee, S.; Zhou, J.; Tongay, S.; Ji, J.; Neaton, B.; Wu, J. *Nano Lett.* **2014**, *14*, 5097–5103.

(30) Wan, K.-T.; Mai, Y.-W. *Acta Metall. Mater.* **1995**, *43* (11), 4109–4115.

(31) Boddeti, N. G.; Koenig, S. P.; Rong, L.; Xiao, J.; Bunch, J. S.; Dunn, M. L. *J. Appl. Mech.* **2013**, *80* (4), 040909.

(32) Deng, S.; Gao, E.; Xu, Z.; Berry, V. *ACS Appl. Mater. Interfaces* **2017**, *9*, 7812–7818.

(33) Cao, Z.; Wang, P.; Gao, W.; Tao, L.; Suk, J. W.; Ruoff, R. S.; Akinwande, D.; Huang, R.; Liechti, K. M. *Carbon* **2014**, *69*, 390–400.

(34) Suk, J. W.; Na, S. R.; Stromberg, R. J.; Stauffer, D.; Lee, J.; Ruoff, R. S.; Liechti, K. M. *Carbon* **2016**, *103*, 63–72.

(35) Zong, Z.; Chen, C.; Dokmeci, M. R.; Wan, K. *J. Appl. Phys.* **2010**, *107*, 026104.

(36) Akinwande, D.; Brennan, C. J.; Bunch, J. S.; Egberts, P.; Felts, J. R.; Gao, H.; Huang, R.; Kim, J. S.; Li, T.; Li, Y.; Liechti, K. M.; Lu, N.; Park, H. S.; Reed, E. J.; Wang, P.; Yakobson, B. I.; Zhang, T.; Zhang, Y. W.; Zhou, Y.; Zhu, Y. *Extrem. Mech. Lett.* **2017**, *13*, 42–72.

(37) Wang, P.; Liechti, K. M.; Huang, R. *J. Appl. Mech.* **2016**, *83* (7), 071002.

DOI: 10.1021/acs.nanolett.7b01735
Nano Lett. XXXX, XXX, XXX–XXX

(38) Shull, K. R. *Mater. Sci. Eng., R* **2002**, *36*, 1−45.
(39) Israelachvili, J. N. *Intermolecular and Surface Forces*; Academic Press, 2011.
(40) Chen, Y. L.; Helm, C. A.; Israelachvili, J. N. *J. Phys. Chem.* **1991**, *95*, 10736−10747.
(41) Yu, Y.; Sanchez, D.; Lu, N. *J. Mater. Res.* **2015**, *30* (18), 2702−2712.
(42) Maugis, D.; Barquins, M. *J. Phys. D: Appl. Phys.* **1978**, *11*, 1989−2023.
(43) de Gennes, P. G. *Rev. Mod. Phys.* **1985**, *57* (3), 827−863.
(44) Kim, S.; Choi, G. Y.; Ulman, A.; Fleischer, C. *Langmuir* **1997**, *13* (25), 6850−6856.
(45) Tian, K.; Gosvami, N. N.; Goldsby, D. L.; Liu, Y.; Szlufarska, I.; Carpick, R. W. *Phys. Rev. Lett.* **2017**, *118*, 1−6.
(46) Israelachvili, J.; Berman, A. *Isr. J. Chem.* **1995**, *35*, 85−91.
(47) Qian, L.; Yu, B. *Adhesion Hysteresis. Encyclopedia of Tribology* **2013**, 29−32.
(48) Shi, Z.; Lu, H.; Zhang, L.; Yang, R.; Wang, Y.; Liu, D.; Guo, H.; Shi, D.; Gao, H.; Wang, E.; Zhang, G. *Nano Res.* **2012**, *5* (2), 82−87.
(49) Liu, X.; Suk, J. W.; Boddeti, N. G.; Cantley, L.; Wang, L.; Gray, J. M.; Hall, H. J.; Bright, V. M.; Rogers, C. T.; Dunn, M. L.; Ruoff, R. S.; Bunch, J. S. *Adv. Mater.* **2014**, *26*, 1571−1576.
(50) Algara-Siller, G.; Lehtinen, O.; Wang, F. C.; Nair, R. R.; Kaiser, U.; Wu, H. A.; Geim, A. K.; Grigorieva, I. V. *Nature* **2015**, *519*, 443−445.
(51) Dollekamp, E.; Bampoulis, P.; Poelsema, B.; Zandvliet, H. J. W.; Kooij, E. S. *Langmuir* **2016**, *32*, 6582−6590.

DOI: 10.1021/acs.nanolett.7b01735
Nano Lett. XXXX, XXX, XXX−XXX